PHYSICAL REVIEW E **75**, 055302(R) (2007)

# Nonlinear convection in rotating systems: Slip-stick three-dimensional traveling waves

Keke Zhang,[1,*] Xinhao Liao,[1] Xiaoya Zhan,[2] and Rixiang Zhu[3]
[1]*Shanghai Astronomical Observatory, Chinese Academy of Sciences, Shanghai 200030, China*
[2]*Department of Mathematical Sciences, University of Exeter, EX4 4QE, United Kingdom*
[3]*Institute of Geology and Geophysics, Chinese Academy of Sciences, Beijing 100029, China*
(Received 27 January 2007; published 23 May 2007)

We investigate convection in a fluid channel uniformly heated from below and rotating about a vertical axis. When the width of the channel is moderate, convective instabilities are characterized by two three-dimensional traveling waves having the same frequency and wave number but traveling in opposite directions with different spatial structures. This Rapid Communication demonstrates that neither the progradely nor the retrogradely traveling wave is physically realizable in the vicinity of the instability threshold. The nature of convection is marked by nonlinear interactions of the two oppositely traveling three-dimensional waves which interfere strongly, leading to either vacillating or stationary convective flows.

DOI: 10.1103/PhysRevE.75.055302 PACS number(s): 47.20.Bp

## I. INTRODUCTION

As a consequence of rotational effects, convective instability and its primary bifurcation in many rotating systems are in the form of either progradely or retrogradely traveling waves. In rotating spheres or spherical shells, the primary bifurcation takes the form of progradely traveling waves of constant amplitude (e.g., [1–4]). In rotating annuli heated from the sidewall with the sloping top and bottom ends, weakly nonlinear convection is described by steadily traveling waves whose direction depends on the curvature of the ends (e.g., [5–8]). In rotating cylinders heated from below, the primary convection near the instability threshold also takes the form of steadily traveling waves of constant amplitude (e.g., [9–13]). Generally speaking, the primary bifurcation from convective instabilities in those rotating systems is characterized by a single traveling wave that has constant amplitude and propagates in a specific direction.

Convection in a fluid channel uniformly heated from below and rotating about a vertical axis, first studied by Davies-Jones and Gilman [14], is fundamentally different. For a rotating Bénard layer in the presence of two vertical sidewalls, the effect of the sidewalls not only destabilizes convection but also produces two oppositely traveling waves with the same frequency and wave number and rich dynamics [15–17]. Whether or how the two oppositely traveling three-dimensional waves interact nonlinearly remains an important unanswered question. An unusual feature of the problem is that the role played by the aspect ratio $\Gamma$, the width to depth of the channel, in linear solutions is quite different from that in nonlinear solutions. While linear solutions are nearly unaffected by the value of $\Gamma$, nonlinear solutions are critically dependent upon the size of $\Gamma$. For moderately small $\Gamma$, the two oppositely traveling waves always interfere nonlinearly and intensively, leading to a primary bifurcation that fundamentally differs from those in spherical or cylindrical or planar geometries. It should be noted that the strong nonlinear interaction cannot occur in a full circular annulus when the inner cylinder is not sufficiently large [18]. This Rapid Communication reports a new convection phenomenon in connection with these two oppositely traveling, nonlinearly interactive, three-dimensional waves in rotating fluid systems.

## II. MATHEMATICAL FORMULATION

We consider convection in a Boussinesq fluid with constant thermal diffusivity $\kappa$, thermal expansion coefficient $\alpha$ and kinematic viscosity $\nu$ in an annular channel of depth $d$ and width $\Gamma d$. The geometry of the problem is shown in Fig. 1. The vertical coordinate is given by $z$, inward radial coordinate by $y$, and azimuthal coordinate by $x$. A cross section of the annular channel is then in the $yz$ plane. By assuming the radius of the annulus is much larger than the width of the annular channel, the effect of the annular curvature is neglected ([14,19]). The fluid channel rotates uniformly with a constant angular velocity $\Omega\hat{\mathbf{k}}$ in the presence of vertical gravity $\mathbf{g}=-g_0\hat{\mathbf{k}}$, where $\hat{\mathbf{k}}$ is a vertical unit vector. As in the Rayleigh-Bénard problem, the channel is uniformly heated from below to maintain an unstable vertical temperature gra-

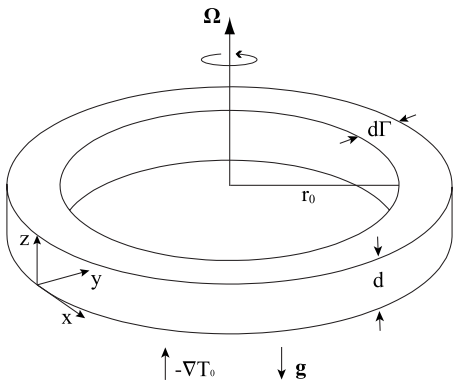


FIG. 1. Geometry of a rotating annular channel whose cross section is defined by $0 \le y \le \Gamma d$, $0 \le z \le d$ with $x$ parallel to the walls of the channel.

*On leave from Department of Mathematical Sciences, University of Exeter, EX4 4QE, UK; electronic address: kzhang@ex.ac.uk

 

dient $\nabla\Theta_0=-\beta\hat{\mathbf{k}}$, where $\beta$ is a positive constant. The convection problem is governed by the three dimensionless equations

$$\frac{\partial \mathbf{u}}{\partial t}+\mathbf{u}\cdot\nabla\mathbf{u}+\mathrm{Ta}^{1/2}\hat{\mathbf{k}}\times\mathbf{u}=-\nabla p+R\Theta\hat{\mathbf{k}}+\nabla^2\mathbf{u}, \quad (1)$$

$$\mathrm{Pr}\left(\frac{\partial\Theta}{\partial t}+\mathbf{u}\cdot\nabla\Theta\right)=\mathbf{u}\cdot\hat{\mathbf{k}}+\nabla^2\Theta, \quad (2)$$

$$\nabla\cdot\mathbf{u}=0, \quad (3)$$

where $\Theta$ represents the dimensionless deviation of the temperature from its conducting state $\Theta_0$, $p$ is the total pressure, and $\mathbf{u}$ is the three-dimensional velocity field $\mathbf{u}=(u_x,u_y,u_z)$ with the corresponding unit vectors $(\hat{\mathbf{i}},\hat{\mathbf{j}},\hat{\mathbf{k}})$. The problem is characterized by three nondimensional parameters, the Rayleigh number $R$, the Prandtl number Pr, and the Taylor number Ta. As in previous studies (e.g., [14,20]), we shall assume conducting and stress-free conditions at the top and bottom and insulating and nonslip conditions at the sidewalls.

We express the velocity $\mathbf{u}$ as a sum of poloidal ($\Phi$) and toroidal ($\Psi$) vectors

$$\mathbf{u}=\nabla\times\nabla\times[\Phi(x,y,z,t)\hat{\mathbf{j}}]+\nabla\times[\Psi(x,y,z,t)\hat{\mathbf{j}}]. \quad (4)$$

Making use of this expression and applying $\hat{\mathbf{j}}\cdot\nabla\times$ and $\hat{\mathbf{j}}\cdot\nabla\times\nabla\times$ onto Eq. (1), we can derive, from Eqs. (1) and (2), three independent scalar equations

$$\left(\nabla^2-\frac{\partial^2}{\partial y^2}\right)\left(\frac{\partial\Psi}{\partial t}-\mathrm{Ta}^{1/2}\frac{\partial\Phi}{\partial z}-\nabla^2\Psi\right)-R\frac{\partial\Theta}{\partial x}=\hat{\mathbf{j}}\cdot\nabla\times(\mathbf{u}\cdot\nabla\mathbf{u}), \quad (5)$$

$$\left(\nabla^2-\frac{\partial^2}{\partial y^2}\right)\left(\frac{\partial\nabla^2\Phi}{\partial t}+\mathrm{Ta}^{1/2}\frac{\partial\Psi}{\partial z}-\nabla^4\Phi\right)-R\frac{\partial^2\Theta}{\partial y\,\partial z}=-\hat{\mathbf{j}}\cdot\nabla\times\nabla\times(\mathbf{u}\cdot\nabla\mathbf{u}), \quad (6)$$

$$\left(\mathrm{Pr}\frac{\partial}{\partial t}-\nabla^2\right)\Theta-\frac{\partial^2\Phi}{\partial y\,\partial z}-\frac{\partial\Psi}{\partial x}=-\mathrm{Pr}(\mathbf{u}\cdot\nabla\Theta). \quad (7)$$

The boundary conditions at the stress-free, conducting top and bottom are

$$\Psi=\frac{\partial^2\Psi}{\partial z^2}=\frac{\partial\Phi}{\partial z}=\frac{\partial^3\Phi}{\partial z^3}=\Theta=0 \quad \text{at} \quad z=0,1, \quad (8)$$

while on the no-slip, insulating sidewalls we require that

$$\Psi=\Phi=\frac{\partial\Phi}{\partial y}=\frac{\partial\Theta}{\partial y}=0 \quad \text{at} \quad y=0,\Gamma. \quad (9)$$

We shall first perform the stability analysis of linearized versions of Eqs. (5)–(7) and then solve the fully nonlinear equations.

## III. INSTABILITY AND BIFURCATION

There exist important spatial symmetries in the governing equations (5)–(7) subject to the conditions (8) and (9). Consider the linear solutions at the onset of convection. Equations (5)–(7) with the boundary conditions (8) and (9) are invariant under the azimuthal translation and reflections with respect to the middle vertical plane $y=1/2$ and to a cross-section plane, say $x=0$. In other words, if

$$[\Phi(x,y,z,t),\Psi(x,y,z,t),\Theta(x,y,z,t)]$$

is a solution to Eqs. (5)–(7), then

$$[\Phi(-x,\Gamma-y,z,t),\Psi(-x,\Gamma-y,z,t),-\Theta(-x,\Gamma-y,z,t)]$$

is also a solution. This implies that there always exist two oppositely traveling three-dimensional waves with the same frequency and wave number but different spatial structures at the onset of convection: one propagates in the retrograde direction (the negative $x$ direction)

$$[\Psi,\Phi,\Theta]_1=[\Psi(y)\sin\pi z,\Phi(y)\cos\pi z,\Theta(y)\sin\pi z]e^{i(ax+\omega t)}, \quad (10)$$

where $a$ is the azimuthal wave number which is henceforth assumed to be positive $a>0$ and $\omega$ denotes the frequency, while the other travels in the prograde direction (the positive $x$ direction)

$$[\Psi,\Phi,\Theta]_2=[\Psi^*(\Gamma-y)\sin\pi z,\Phi^*(\Gamma-y)\cos\pi z,-\Theta^*(\Gamma-y)\sin\pi z]e^{i(ax-\omega t)}. \quad (11)$$

Here $f^*$ denotes the complex conjugate of $f$. For $\mathrm{Ta}\gg 1$ with $\Gamma\geq O(\mathrm{Ta}^{-1/6})$, the two traveling waves tend to concentrate in the vicinities of the two sidewalls with typical radial scale $O(\mathrm{Ta}^{-1/6})$. For example, there exist two most unstable convection modes for $\mathrm{Ta}=10^6$ and $\Gamma=0.5$ at $\mathrm{Pr}=7.0$ (water at room temperature). They correspond to two oppositely traveling waves: the retrograde mode concentrating at the outer sidewall ($y=0$) is described by the critical Rayleigh number $R_c=3.52\times10^4$ with the critical wave number $a_c=4.1517$ and the critical frequency $\omega_c=4.135$, while the prograde mode concentrating at the inner sidewall ($y=\Gamma$) is characterized by $R_c=3.52\times10^4$ with $a_c=4.1517$ and $\omega_c=-4.135$. The structure of both the most unstable modes is depicted in Fig. 2.

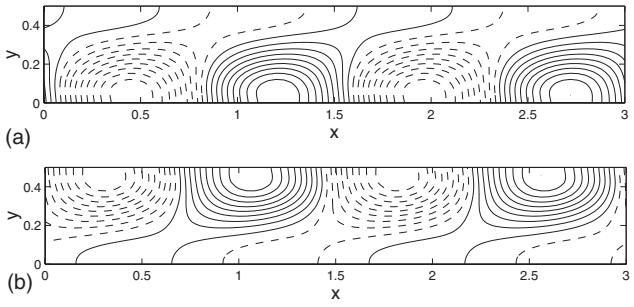


FIG. 2. Linear traveling wave solutions for $\Gamma=0.5$, $\mathrm{Pr}=7$, and $\mathrm{Ta}=10^6$ with $R_c=3.52\times10^4, a_c=4.1517$: (a) contours of $\Theta$ at $z=1/2$ for the retrograde mode ($\omega=4.135$); (b) $\Theta$ at $z=1/2$ for the prograde mode ($\omega=-4.135$).

A distinct feature of the problem is the role played by the aspect ratio $\Gamma$ in determining the nature of nonlinear solutions. For the linear problem, traveling wave solutions are

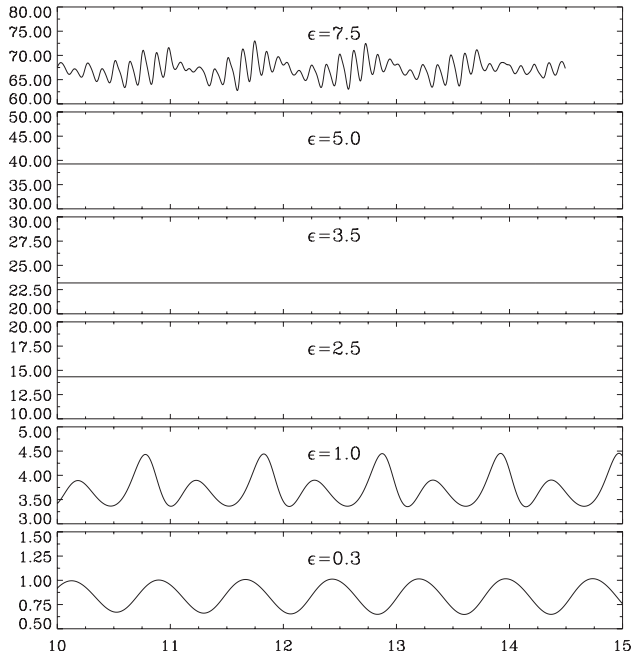


FIG. 3. Kinetic energies of nonlinear convection at six different values of $\varepsilon$ for $\Gamma=0.5$, Pr=7, and $\mathrm{Ta}=10^6$.

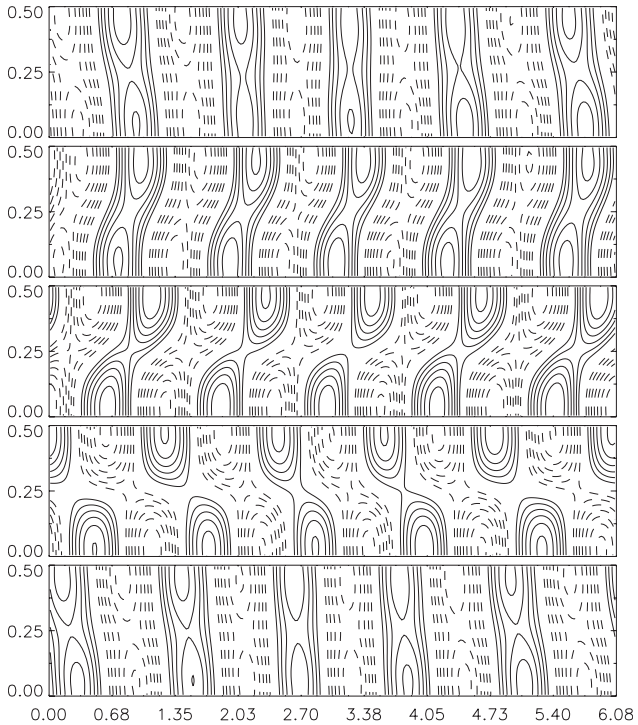


FIG. 4. Contours of $\Theta$ at $z=1/2$ for convection for $\Gamma=0.5$, Pr=7, $\mathrm{Ta}=10^6$, $\varepsilon=0.3$ at five different instants in the one oscillation period.

hardly affected by the size of $\Gamma$ as long as $\Gamma > O(\mathrm{Ta}^{-1/6})$ with $\mathrm{Ta} \gg 1$. Parameters for the convective instabilities such as the critical Rayleigh number and critical wave number remain nearly unchanged for any value of $\Gamma$ in the regime $\Gamma \geq O(\mathrm{Ta}^{-1/6})$. Moreover, the profiles of linear solutions for different values of $\Gamma$ are almost identical to that shown in Fig. 2 apart from extra motionless regions. For the nonlinear problem, however, convection is critically dependent upon the size of $\Gamma$. For $\Gamma \gg O(\mathrm{Ta}^{-1/6})$, the two traveling waves are decoupled and may be studied independently (e.g., [12,13]). For $\Gamma = O(\mathrm{Ta}^{-1/6})$, the two waves traveling in the opposite directions with the same wave number and frequency interfere destructively or constructively, creating a unique nonlinear dynamics in rotating convection. In this case, there are four possible scenarios for nonlinear convection in the vicinity of the threshold: (i) a retrogradely steadily traveling wave of constant amplitude, (ii) a progradely steadily traveling wave of constant amplitude, (iii) a standing-wave nonlinear convection and (iv) a vacillating convection resulting from strong nonlinear interaction between the two traveling waves. Since the two three-dimensional waves have different spatial structures, for instance, $\Phi(y) \neq \Phi^*(\Gamma - y)$ and $\Theta(y) \neq \Theta^*(\Gamma - y)$, the third possibility, that of a nonlinear standing-wave solution, can be ruled out.

Analytical studies for nonlinear convection involving two three-dimensional waves appears to be formidable since even linear solutions are highly complicated and very lengthy. We hence choose to tackle the nonlinear problem via direct three-dimensional numerical simulations. In an attempt to unveil the nature of the primary bifurcation from convective instabilities, we introduce $\epsilon = (R - R_c)/R_c$ to measure the degree of supercriticality and then simulate nonlinear convection gradually from small to moderate values of $\epsilon$. Figure 3 shows kinetic energies of nonlinear convection for several values of $\epsilon$ for $\Gamma=0.5$, Pr=7.0, and $\mathrm{Ta}=10^6$ with the critical Rayleigh number $R_c = 3.52 \times 10^4$. It should be noted that the transient behaviors from arbitrary initial conditions are not shown in Fig. 3 since the nonlinear solutions are robust and not affected by the precise form of initial conditions used in the simulations. It is found that neither the retrogradely traveling wave nor the progradely traveling wave is separately physically realizable. In the weakly nonlinear regime $0 < \epsilon \leq 1$, two traveling waves having the same wave number and frequency traveling in opposite directions always interact nonlinearly. This will be referred to as two slipping oppositely traveling waves. Dependent upon the relative phases of the two waves at any instant, the interference can be destructive or constructive, resulting in time-dependent vacillating convection. Figure 4 depicts the profiles of the vacillating convection at a number of different instants for $\epsilon=0.3$. When the phase of the two waves is the same (top and bottom panel in Fig. 4), the amplitude of the nonlinear flow reaches a minimum while it attains a maximum when they are out of the phase (middle panel in Fig. 4).

When nonlinear effects are sufficiently strong in $1 < \epsilon < 6$, however, the two oppositely traveling and nonlinearly interactive waves are combined to form a stationary flow representing the secondary bifurcation. This will be referred to as two stuck oppositely traveling waves. The structure of three stationary nonlinear solutions for $\epsilon = 2.5, 3.5, 5.0$ is depicted in Fig. 5 and their kinetic energies are shown in Fig. 3. The profile for $\epsilon=2.5$ (top panel in Fig. 5) is largely similar to that shown in Fig. 4 (top panel) at the instant when the two oppositely traveling waves have nearly the same phase. When $\epsilon$ increases further, the phase differ-

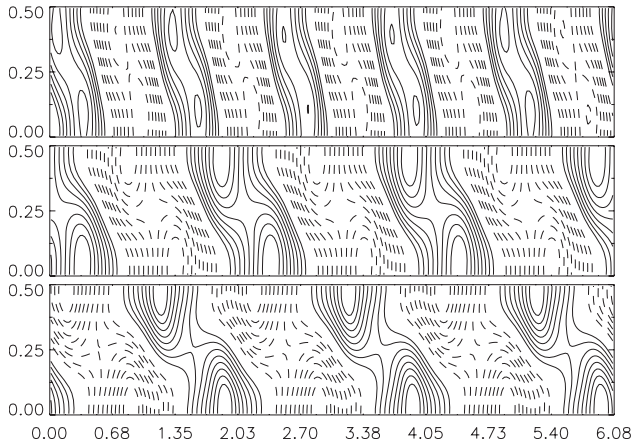


FIG. 5. Contours of $\Theta$ at $z=1/2$ for nonlinear stationary convection for $\Gamma=0.5$, $\mathrm{Pr}=7$, and $\mathrm{Ta}=10^6$ for $\varepsilon=2.5$ (top panel), $\epsilon=3.5$ (middle panel), and $\epsilon=5.0$ (bottom panel).

ence becomes greater, as clearly shown in Fig. 5 (middle and bottom panels). However, they still stick together: the resulting nonlinear convection remains stationary. Our numerical simulations suggest that the stationary convection produced by two stuck oppositely traveling waves is the only stable solution in the regime $1<\epsilon<6$. Nonlinear convection becomes oscillatory, as shown in Fig. 3, when the supercritical Rayleigh number increases to $\epsilon=7.5$.

## IV. CONCLUDING REMARKS

We have shown that neither progradely nor retrogradely traveling waves can represent a stable nonlinear state in the vicinity of the threshold when the width of the channel is moderate. The primary bifurcation from convective instabilities is always marked by two three-dimensional waves that travel in opposite directions and interfere nonlinearly, either destructively or constructively, leading to a vacillating convective flow. The two slipping traveling waves become stuck together when nonlinear effects become sufficiently strong in the regime $\epsilon=O(1)$, leading to a secondary bifurcation in the form of stationary convection representing two stuck oppositely traveling waves.

This Rapid Communication represents the first study of nonlinear convection in rotating fluid systems in which the flow is characterized by strong nonlinear interactions between two oppositely traveling three-dimensional waves with the same frequencies and wave numbers but different spatial structures. We have only so far tackled the problem of nonlinear convection through fully three-dimensional numerical simulations. An analytical theory describing nonlinear convection in the form of slipping or stuck oppositely traveling three-dimensional waves remains a challenging task.

## ACKNOWLEDGMENTS

K.Z. is supported by UK NERC, Leverhulme Trust, and PPARC grants. X.L. and R.Z. are supported by NSFC and CAS grants. K.Z. would like to thank F. H. Busse for helpful discussions. The numerical computation was supported by SSC.

[1] K. Zhang, J. Fluid Mech. **236**, 535 (1992).
[2] F. M. Al-Shamali, M. H. Heimpel, and J. M. Aurnou, Geophys. Astrophys. Fluid Dyn. **98**, 153169 (2004).
[3] A. M. Dormy, A. M. Soward, C. A. Jones, D. Jault, and P. Cardin, J. Fluid Mech. **501**, 43 (2004).
[4] K. Zhang, X. Liao, and F. H. Busse, J. Fluid Mech. **578**, 371 (2007).
[5] M. A. Azouni, E. W. Bolton, and F. H. Busse, Geophys. Astrophys. Fluid Dyn. **34**, 301317 (1986).
[6] E. Plaut and F. H. Busse, J. Fluid Mech. **464**, 345363 (2002).
[7] C. A. Jones, J. Rotvig, and A. Abdulrahman, Geophys. Res. Lett. **30**, 1 (2003).
[8] J. Rotvig and C. A. Jones, J. Fluid Mech. **567**, 117 (2006).
[9] F. Zhong, R. Ecke, and V. Steinberg, Phys. Rev. Lett. **67**, 2473 (1991).
[10] H. F. Goldstein, E. Knobloch, I. Mercader, and M. Net, J. Fluid Mech. **248**, 583 (1993).
[11] J. Herrmann and F. H. Busse, J. Fluid Mech. **255**, 183 (1993).
[12] E. Y. Kuo and M. C. Cross, Phys. Rev. E **47**, R2245 (1993).
[13] E. Plaut, Phys. Rev. E **67**, 046303 (2003).
[14] R. P. Davies-Jones and P. A. Gilman, J. Fluid Mech. **46**, 65 (1971).
[15] X. Liao, K. Zhang, and Y. Chang, Geophys. Astrophys. Fluid Dyn. **99**, 445 (2005).
[16] Y. Chang, X. Liao, and K. Zhang, Geophys. Astrophys. Fluid Dyn., **100**, 215 (2006).
[17] X. Zhan, R. Zhu, and X. Liao, Phys. Earth Planet. Inter. **159**, 96 (2006).
[18] E. Serre, E. Crespo del Arco, and F. H. Busse, Transition to Choatic Patterns in Rayleigh-Bénard Convection in Rotating Cylinders, in *Nonlinear Dynamics in Fluids*, edited by F. Marqués and A. Meseguer (CIMNE, Barcelona, 2003), pp. 138–140.
[19] P. A. Gilman, J. Fluid Mech. **57**, 381 (1973).
[20] F. H. Busse, J. Fluid Mech. **537**, 145 (2005).